

# Stable solar cycles

Kim Chol-jun

*Faculty of Physics, Kim Il Sung University, DPR Korea*

email address: cj.kim@ryongnamsan.edu.kp

## Abstract

The question on the long-term solar cycles is still open. I choose the stable solar cycles in terms of the sampling and differencing stability in samplogram, the time stability or stationarity in wavelet scalogram and the modulation analysis. The short-term solar cycles are also little known due to the strong randomness of solar activity. I found the stable cycles near to the orbital cycles of all major planets upto the Saturn. This may imply a possible planetary forcing of solar activity.

## 1 Introduction

Solar activity is considered to be a non-stationary and stochastic process. However, the 11-yr Schwabe cycle implies that the solar activity should be many periodic. The difficulty to predict the 11-yr solar cycle may be related to the unknown long-term solar cycles (Petrovay, 2010). There have not been discovered any significant cycle even of short period except the Dicke's 27-day cycle (Hathaway, 2015).

The reconstruction of the past solar activity, based on the inspection of cosmogenic radionuclides such as  $^{14}\text{C}$  extracted from the tree ring and  $^{10}\text{Be}$  measured from the ice core (Solanki et al., 2004; Steinhilber et al., 2012; Wu et al., 2018), allows us to analyze the long-term solar cycles: the Gleissberg (88-yr), Suess/de Vries (208-yr) and Hallstatt cycles ( $\sim 2400$ -yr) show significant appearances in most analyses (Beer, Tobias & Weiss, 2018; Chol-jun & Jik-su, 2020; Usoskin et al., 2016) and the Eddy ( $\sim 1000$ -yr) and unnamed  $\sim 350$ -yr as well as  $\sim 500$  and  $\sim 710$ -yr cycles have been reported, though they are less significant (Usoskin, 2008).

According to Chol-jun (2020), a mere significance of peak in spectrum cannot tell us whether this peak represents a true or spurious cycle. A non-iterative separation between the grand extremes can make a spurious but significant peak in spectrum. In this paper we apply the sampling and differencing (SnD) stability analysis to inspect the solar activity. However, even in this way we cannot remove the all spurious cycles. To compensate this drawback, we use a new method: a time stability or stationarity analysis of cycle in wavelet analysis, which shows how long the local cycle maintain in the scalogram. This method comes from the idea that the non-iterative separation, i.e. time-local cycle, can make a peak in the spectrum.

Another way is performed in this paper: the modulation analysis. The so-called Hallstatt modulation of the Suess/de Vries cycle has been announced many times. This is an argument of existence of not only the former cycle but the latter one. The relation is a natural property of the object. We can obtain the modulation in analyzing the waveform of the cycle or scale in the wavelet scalogram. The modulation gives us another possibility to gain the stable cycles.

A spurious cycle in a random signal should become different in another realization of the signal. We compare various datasets of solar activity: the reconstructions during the Holocene and modern official records of the solar activity.

## 2 The stable long-term solar cycles

### 2.1 The sampling and differencing stability in the samplogram

The samplogram shows the sampling and differencing (SnD) stability of the cycle. We inspect the reconstructed solar activity during the Holocene with two datasets: the reconstructed sunspot number (RSSN)<sup>1</sup> and the reconstruction of total solar irradiance (RTSI)<sup>2</sup>.

<sup>1</sup>The dataset is available through the MPS sun-climate web-page at [https://www2.mps.mpg.de/projects/sun-climate/data/SN\\_composite.txt](https://www2.mps.mpg.de/projects/sun-climate/data/SN_composite.txt). The dataset covers the period from 6755 B.C. to A.D. 1885 by the decadal interval. See also Wu et al. (2018).

<sup>2</sup>The dataset is available through the NOAA web-page at [https://www1.ncdc.noaa.gov/pub/data/paleo/climate\\_forcing/solar\\_variability/](https://www1.ncdc.noaa.gov/pub/data/paleo/climate_forcing/solar_variability/). The dataset covers the period from 7439 B.C. to A.D. 1977 by the 22-yr interval. See also Steinhilber et al. (2012).

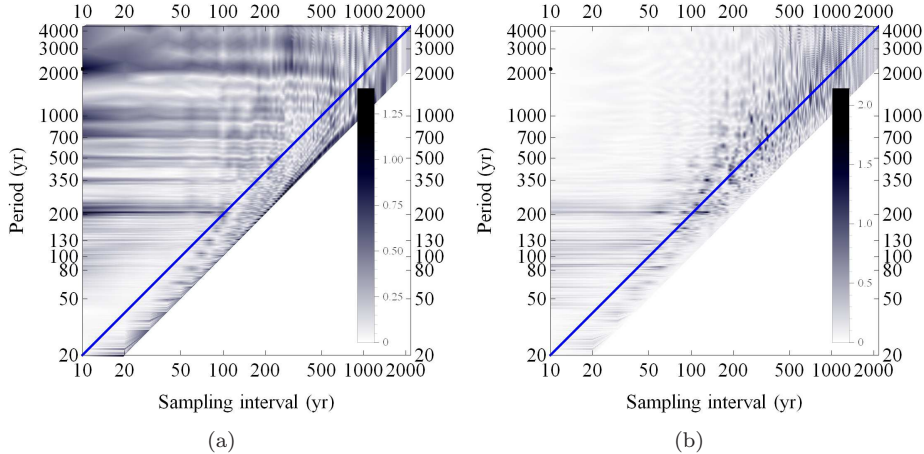


Figure 1: The samplogram and D1-samplogram for the RSSN. (a) The samplogram shows how the power spectrum changes when the sampling interval increases in the average down-sampling and (b) D1-samplogram is the samplogram for the 1-st order differences. The blue diagonal stands for the Nyquist sampling. The right oblique boundary of the diagram shows the Fourier limit where the sampling interval is equal to the cycle considered.

We perform the samplogram analysis for the both datasets. In the samplogram the sampling-stable cycle appears in form of a ridge, which is an extension of peak while the sampling interval increasing (Fig. 1a). We can also examine the differencing stability of the cycles. The difference series (or the differences) that is consisted from differences between the adjacent data points in the time series can be evaluated also by the samplogram, which we call the  $Dl$ -samplogram, where  $l$  is the differencing order. We compare the ridges or peaks in the (D0-) samplogram with them in the  $Dl$ -samplogram to check the differencing stability of cycle. When the sampling interval is increasing in the averaging down-sampling, the shorter cycles are depressed and the longer cycles are amplified (Chol-jun, 2020). On the other hand, by the differencing, the longer cycles are depressed and shorter cycles are amplified, because the amplitude is multiplied by the frequency of cycle. The more the differencing order  $l$  increases, we can see that the shorter cycles are accented in the  $Dl$ -samplogram. Figure 1 shows samplogram and D1-samplogram for the RSSN. The two ridges (2200 and 3300 yr) in both datasets seem commonly to stand for the single Hallstatt cycle. The reason for this will be explained below: the length of the Hallstatt cycle is varying.

Figure 2(a) shows only the peaks of power spectra for the various differences (from 0 to 3-rd order where 0 stands for the raw time series) of the RSSN. We check which cycle has the quadruple peak points of the 0 to 3-rd order differences continued to the its Nyquist sampling. At a given sampling, the peak point of the given cycle might be a bit displaced in the frequency domain in the discrete Fourier transform (DFT) where the every cycle must be represented only by an integer frequency index. To show the tolerance of the peak points due to the rounding of the decimal frequency index, we introduced the error bars in Fig. 2(a). In other words, the error bar means the range of period corresponding to the given frequency index  $\pm 0.5$ . Some cycles (e.g. a couple of 349.6 and 377.5 yr) have different ridges in the samplogram (that is, 0-th order), but have the common ridges or peaks in the D-samplograms, which implies that those cycles are no more than the sidewaves for a single cycle that has a frequency variance.

We use the aforementioned error bar to evaluate the SnD stability of cycles. We consider a period in the ordinate of samplogram. And increasing the sampling interval on the abscissa, we count how many times this period belongs to the error bars in the samplogram. This counting is limited upto the Nyquist sampling, as beyond the Nyquist sampling there appear the aliasing ridges. The counted number is divided by the number of sampling step on abscissa upto the Nyquist sampling for the considered period. We can think this ratio to represent the sampling stability of the period. To evaluate the differencing stability, we calculate the sampling stability of the period in the various D-samplograms (for example, from D0 to D3-samplograms) and evaluate their average. We can define this value as the SnD stability of the cycle:

$$\text{the SnD stability of a cycle} = \frac{1}{4} \sum_{d=0}^3 \frac{\text{number of samplings involved in any errorbar of the } d\text{-th order peak upto the Nyquist sampling for the cycle}}{\text{number of samplings upto the Nyquist sampling for the cycle}}, \quad (1)$$

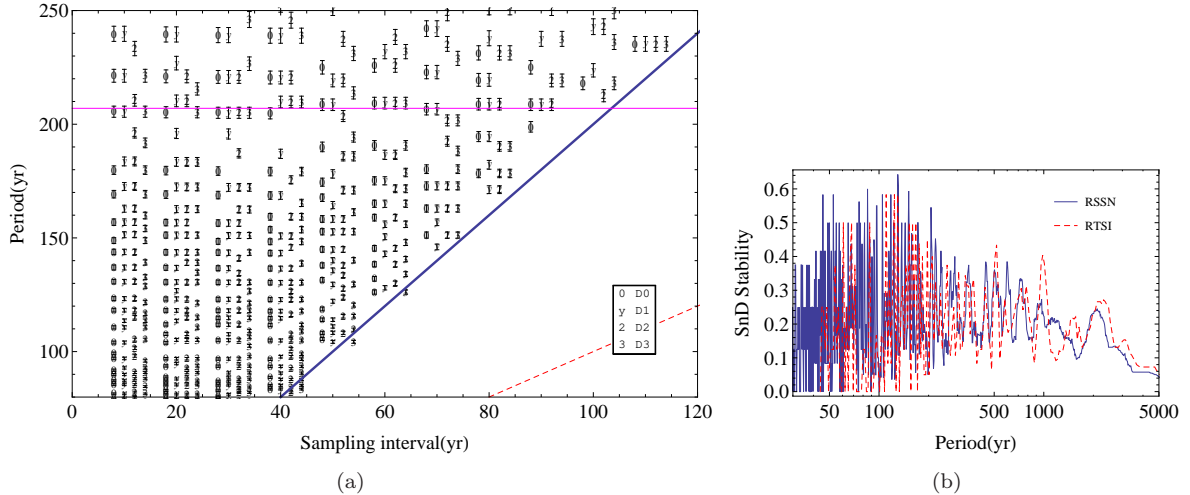


Figure 2: The peaks in the samplogram and D-samplograms (from 1 to 3rd order) of RSSN within the period of 80 to 250 yr (a) and the SnD stability of the cycles for both reconstructed solar activity RSSN and RTSI (b). In (a), the marks “0”, “y”, “2” and “3” stand for the peak points in spectra of the 0-th to 3-rd order differences respectively. The error bars mean the period resolution related to the rounding of the frequency index. The error bars are displaced horizontally from the original peak points to discriminate the peaks of the different orders. The number of crossings between the horizontal line for a cycle and the errorbars can define the SnD stability of the cycle. See the text. The horizontal line stands for the 207-yr cycle, for example. The blue diagonal implies the Nyquist sampling. The aliasing periodicity regions beyond the Nyquist sampling are neglected. the red dotted line stands for the Fourier limit where the period is equal to the sampling interval. In (b) the frequency is given in the similar way as in the wavelet analysis so that the number of voices within an octave for frequency is 100.

where  $d$  is the differencing order, which we limited to 3 for the convenience so  $\frac{1}{4}$  means an average for differencing order, and the sampling stands for the sampling interval. The numerator equals the number of crossings between the horizontal line for the cycle and the errorbars for the  $d$ -th order peaks in Fig. 2 while the denominator is equal to the half cycle divided by the sampling step of the raw dataset. Figure 2(b) shows the SnD stability of cycles in the RSSN and RTSI datasets. In this figure we can see that the period less than 200 yr looks to be very spiky and almost discontinuous, i.e. the stability of the two close periods might be much different. This is because in the short-cycle region there appear many noisy peaks. And another factor is that the short range of sampling interval to the Nyquist sampling is given to check for stability.

To compare with the modern official records of the solar activity, we apply the samplogram to the two yearly datasets: the international SN series (SILSO ISN version 2<sup>3</sup>) and the Group Sunspot Number (GSN) series<sup>4</sup>. We evaluate the SnD stability in samplogram with similar way as above (Fig. 3).

We can find many SnD stable cycles, which correspond to the extremes in the SnD stability. However, we cannot claim that all of those cycles are really true cycles of solar activity. The spurious cycle could appear in the samplogram. We perform other method based on the wavelet analysis.

## 2.2 The time stability or stationarity in the wavelet scalogram

As Chol-jun (2020) indicated, the time-local cycle or intermittent cycle can appear to be stationary cycle spuriously in the spectrum. So we analyze the time stability of the cycle in the time-frequency analysis, i.e. the wavelet analysis. The time stability shows how long the cycle maintains along the time advancement.

In the wavelet scalogram we can find the ridge, which is formed from the peaks corresponding to the time-local cycles. Figure 4 shows the wavelet scalogram for the SSN datasets and ridges of some cycles. For evaluation of the time stability of cycles, we count the number of time points where the peaks for the cycle or scale (the scale stands for the cycle) appear outside the cone of influence (COI, within which the analysis is possibly biased by the effect of edge). And divide this number by the length of the time series. We can define this ratio as the

<sup>3</sup> The dataset is available at [http://www.sidc.be/silso/DATA/SN\\_y\\_tot\\_V2.0.txt](http://www.sidc.be/silso/DATA/SN_y_tot_V2.0.txt). The yearly dataset covers the period from 1700.5 to 2018.5. See also Clette et al. (2014).

<sup>4</sup> The dataset is available at <http://www.sidc.be/silso/groupnumberv3>. The yearly dataset covers the period from 1610.5 to 1995.5 and the monthly dataset covers the period from 1610/01 to 1995/12. See also Hoyt & Schatten (1998).

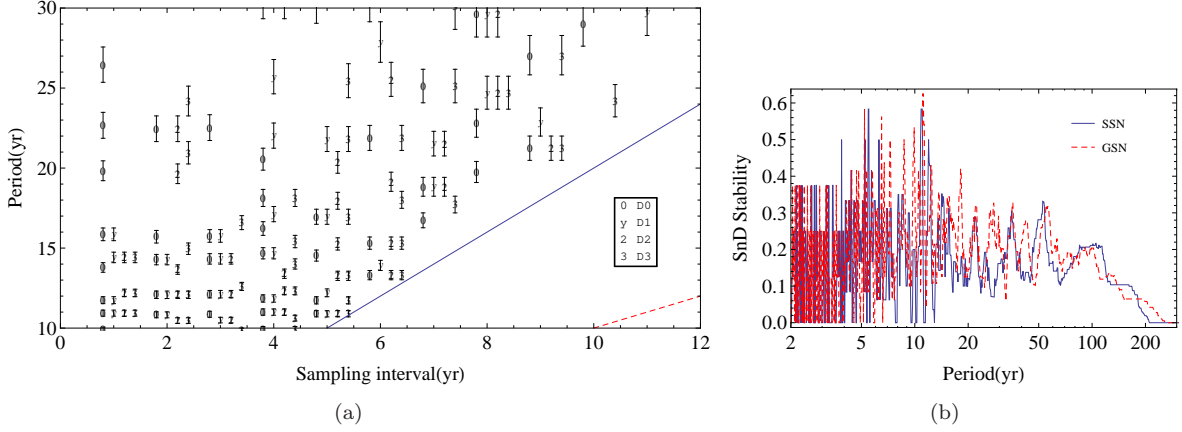


Figure 3: The peaks in the samplogram and D-samplograms (from 1 to 3rd order) for the modern yearly SSN within the period of 10 to 30 yr (a) and the SnD stability of the cycles for the modern yearly SSN and GSN (b). Refer to Fig. 2.

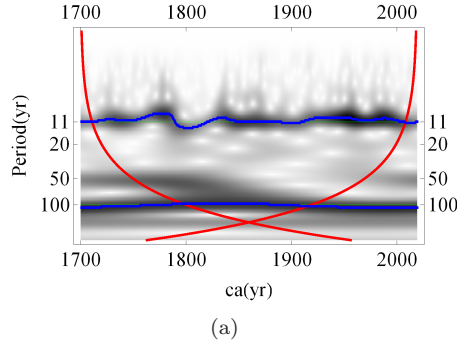


Figure 4: The ridges of the 11 and 100-yr cycles in the modern SSN. The blue curves stand for the ridges and the green horizontal lines for the given cycle. The background density plot shows the wavelet scalogram. The red curves delimit the cone of influence (COI).

time stability (T stability or the stationarity) of the cycle:

$$\text{the T stability of a cycle} = \frac{\text{number of peak points outside COI for the cycle}}{\text{number of time points for the cycle}}, \quad (2)$$

where the numerator equals the number of crossings between the horizontal line for the cycle and all ridges around the cycle in Fig. 4 while the denominator is equal to the time period divided by the time step for the raw dataset. Figure 5 shows the time stability of period for the RSSN, RTSI, SSN and GSN datasets. We can find that the long cycles are stable in spite of that the range outside the COI for the longer cycle is shorter than that for the shorter cycle. This is the reason why we take the length of the time series as the denominator of the time stability rather than the length of range outside the COI. Also this seems to be similar to that the long spurious cycle appears to be stable in the samplogram (Chol-jun, 2020). We can see that the T stable cycles are similar to the SnD stable cycles. This shows that the spurious cycle is originated also from the non-stationarity of signal as said in Chol-jun (2020).

We can see that the doubling cycle of the time step for a dataset appears to be stable. For example, the 20 yr for the RSSN and 44 yr for the RTSI are such cycles. Those cycles are related not with the solar activity, but only with the sampling process so we neglect them. For the RSSN and RTSI datasets, the 1500-yr cycle appears, which seems to have no relation with the 3000-yr cycle because there does not appear the 3000-yr cycle for the RTSI while for the RSSN there appears the 3000-yr cycle. In the samplogram we can find the faint cycle of 1400-1500 yr near the Nyquist sampling. The 1500-yr cycle in RTSI might be related the 1500-yr cycle in the climate change (Bond et al., 1997), but this seems to be too weak. Unfortunately, the Suess/de Vries cycle is not time-stable in the RSSN but rather the 220-yr cycle is time-stable. We think that a period in the wavelet analysis appears a bit different from that in the power spectrum.

There appears no perfect stationary cycle including the 11-yr cycle. We can see the 11-yr cycles are partly stable in the SSN and GSN datasets, which might be due to the period variation such as the Waldmeier effect.

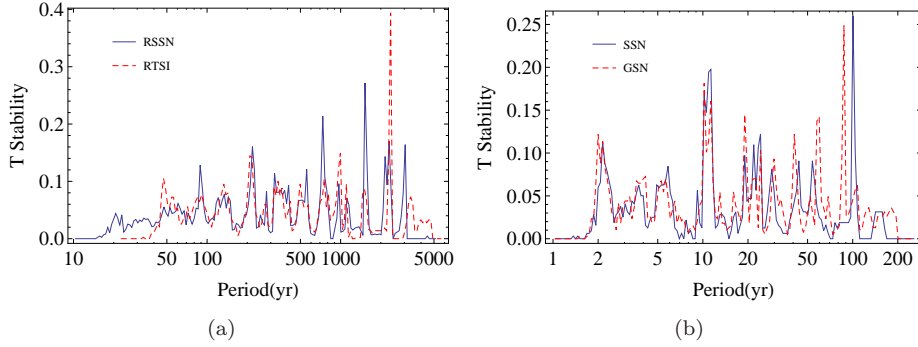


Figure 5: The time stability of period for the RSSN and RTSI (a), SSN and GSN (b). In the wavelet analysis we use the Morlet basis and the number of voices per octave is set 20.

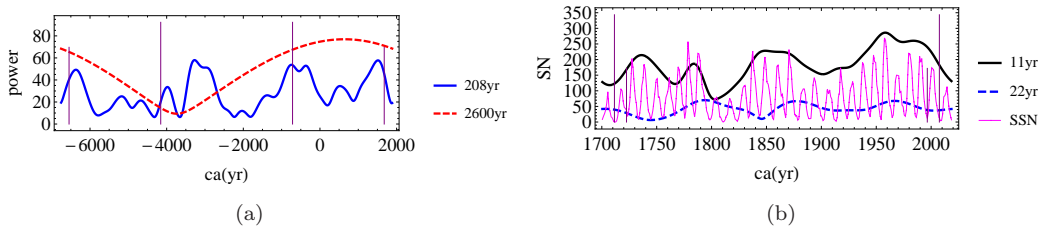


Figure 6: The waveforms of the 208 (blue) and 2600-yr scales (red dashed) for the RSSN (a) and of the 11 (black) and 22-yr scales (blue dashed) for the modern SSN (b) datasets. The thin magenta line stands for the RSSN and SSN variations. The vertical lines mean the cone of influence for the 208 and 2600-yr scales in (a), the 11 and 22-yr scales in the wavelet analysis in (b).

Beside that, the 19, 22, 24 and 29-yr cycles appear stable commonly in the SSN and GSN. What is interesting is the 87 and 128-yr cycles in the GSN dataset, which are the local cycles corresponding to the Gleissberg (88-yr) and Attolini (130-yr) cycles during the Holocene. However, those cycles do not appear in the SSN probably because the length of the SSN dataset may be short.

### 2.3 The modulation analysis

The long-term solar cycles can appear in another form: the modulation. As many authors mentioned, the Suess/de Vries cycle is modulated by the Hallstatt cycle. This implies some cycles may have meaning only as the modulation on other cycles. And this manifests the stable existence of both cycles: the carrier and modulation cycles. We investigate the modulation of cycles by each other. For this, the waveform in wavelet scalogram is used. The waveform shows how the power for the given scale (or cycle) changes with time (Fig. 6). We perform the Fourier analysis for the waveform again and draw the modulation chart for the reconstructed solar activity (Fig. 7a, b). Scanning the aforementioned significant cycles, we can find the several modulation groups commonly appeared in the RSSN<sup>1</sup> and RTSI<sup>2</sup>: the 160 to 230 and 650 to 800-yr scales modulated by the  $\sim 2800$ -yr cycle, the 260 to 340-yr scales modulated by the  $\sim 1500$ -yr cycle, the 160 to 230-yr scales modulated by the  $\sim 700$ -yr cycle, the 20 to 340-yr scales modulated by the  $\sim 500$ -yr cycle. However, the length of modulation cycle for such groups varies. For example, we can see that around 5000-3000 B.C. the power of the Hallstatt cycle is the lowest and its period is estimated to be  $\sim 3200$  yr from separation between adjacent peaks in the waveform for the 208-yr scales (Fig. 6a). However, around A.D. 1000-2000 its power is the highest and its period is  $\sim 2200$  yr. This variation of the Hallstatt cycle is a probable reason of the ridges for 2200 and 3300 yr in Fig. 1. Beside the such common significant modulation groups, there are many miscellaneous modulations (Table 1).

We also analyze the modulations for the modern SSN<sup>3</sup> and GSN<sup>4</sup> datasets (Fig. 7c). Both datasets show several common modulation groups: the 22 to 25-yr scales modulated by the  $\sim 87$ -yr cycle, the 7 to 9-yr scales modulated by the  $\sim 50$ -yr cycle and the 5 to 7-yr scales modulated by the  $\sim 21$ -yr cycle. An interesting modulation here is the modulation of the 22 to 25-yr scales by the  $\sim 90$ -yr cycle. This implies that the Gleissberg cycle of 88 yr could be the modulation cycle of the Hale cycle of 22 yr (Fig. 6b). In fact, we can not find the Gleissberg cycle in the spectrum for the modern SSN records. The  $\sim 90$ -yr-cycle modulation of the  $\sim 22$ -yr scale

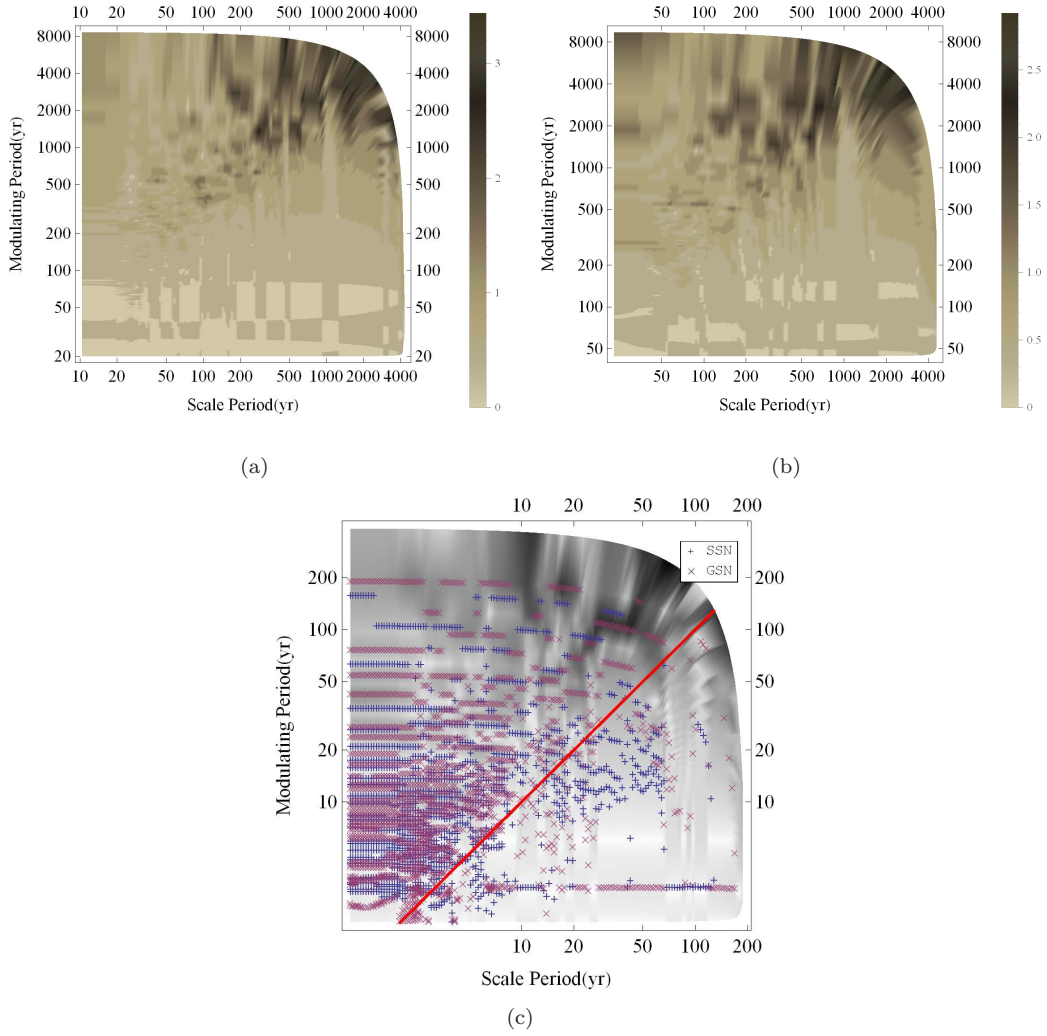


Figure 7: The charts of modulation for the RSSN (a), RTSI (b) datasets and overlay of the modern SSN and GSN datasets (c). The abscissa stands for the carrier cycle and the ordinate stands for the modulating cycle. The top-right curved boundary means the cone of influence. In (c) the background density plot stands for the GSN and marks "+" and "x" stand for the peaks in spectra of the waveform of scales for the SSN and GSN datasets, respectively. The red diagonal stands for the equality between periods of carrier and modulation cycles. The wavelet analysis is performed with the Morlet basis and the number of voices per octave is set 20.

appears commonly in the both datasets of SSN and GSN. This could give the physical interpretation for the Gleissberg cycle. The fact that 88 yr is just 4 times 22 yr would justify this hypothesis. Another argument is that the Gleissberg cycle has no specific modulation during the Holocene (Ma, 2009). There would be no modulation of the modulation itself. However, this is no more than a supposition at now. We have to show if this modulation was stable even during the Holocene. The modulation cycle of the 11-yr cycle is  $\sim 100$  yr for the SSN and  $\sim 120$  yr for the GSN. In fact, the modulation cycles of the 11-yr cycle are different in both datasets, which implies that these cycles are spurious.

## 2.4 Comparison of the spectra between the reconstructed and modern SSN

Solanki et al. (2004) showed that the reconstructed sunspot number series from cosmogenic radionuclides is very similar to the 10-year averaged GSN series. Here we compare the spectra for the reconstructed and modern SSN. For analytic interpretation, we compare the Fourier spectra. We use the semi-analytic formula for the Fourier spectrum in Chol-jun (2020). To do this, we suppose a time series of a multi-cyclic signal:

$$u(r) = \sum_j U_j \cos\left(\frac{2\pi r \Delta t}{T_j} + \phi_j\right), \quad (3)$$

where  $U_j, T_j$  and  $\phi_j$  are the amplitude, period and phase of the  $j$ -th mode of the signal, respectively. And  $\Delta t$  is a time step.  $r$  is the index of point in the time series and runs from 1 to  $N$  that is the length of the time series. The discrete Fourier transform (DFT) of the time series Eq. (3) is approximatedly expressed as

$$v(q) \approx \sum_j \frac{U_j}{2\sqrt{N}} \left\{ \exp(i\phi_j) \exp\left(\frac{2\pi i}{N} q_{0j}\right) \frac{1 - \exp[2\pi i(q + q_{0j})]}{1 - \exp\left[\frac{2\pi i}{N}(q + q_{0j})\right]} \right. \\ \left. + \exp(-i\phi_j) \exp\left(-\frac{2\pi i}{N} q_{0j}\right) \frac{1 - \exp[2\pi i(q - q_{0j})]}{1 - \exp\left[\frac{2\pi i}{N}(q - q_{0j})\right]} \right\}, \quad (4)$$

where  $q_{0j} = N \frac{\Delta t}{T_j}$  is the frequency index of the  $j$ -th mode. The first term in Eq. (4) stands for the aliasing peak in spectrum so this can be neglected at  $q \approx q_{0j}$  where the true peak is supposed to appear. Then the amplitude and phase of the  $j$ -th mode can be determined from the discrete Fourier transform (Eq. 4):

$$U_j \approx \frac{2}{\sqrt{N}} \text{Abs}(v(q_{0j})), \quad (5)$$

$$\phi_j \approx -\text{Arg}(v(q_{0j})) - \frac{2\pi}{N} q_{0j}, \quad (6)$$

where  $\text{Abs}(v(q_{0j}))$  and  $\text{Arg}(v(q_{0j}))$  stand for the absolute value and argument of the  $v(q)$  at  $q = q_{0j}$ .

We compare the amplitudes of the reconstructed SSN<sup>1</sup> and 10-yr averaged modern SSN<sup>3</sup> calculated by Eq. (5). (The value of RSSN is 2 times smaller than the SSN, which we compensate.) In Fig. 8 the decade-averaged modern SSN shows the similar spectrum to the yearly modern SSN and has the  $\sim 30$ ,  $\sim 50$  and  $\sim 100$ -yr peaks. However, we can see a great discrepancy between both spectra of the modern and reconstructed SSN. So we can conclude that the 30, 50 and 100-yr cycles in the modern SSN dataset are not true solar cycles. For example, this cycle might come from a separation between the crests of the other long-term cycles or the random part in the dataset. Fortunately, the spectrum of the modern SSN does not exclude any aforementioned long-term cycle in the RSSN, e.g. the 88 or 130 yr: the spectrum for the modern SSN exceeds that for the RSSN at all periods. This should be reason why we cannot find long-term cycles such as 88 and 130 yr in the modern SSN: those cycles might be embedded into the spectrum for the modern SSN.

The case of the 120 and 200-yr cycles in the GSN are similar. We cannot conclude that these cycles are the true solar cycles. In fact, the 120-yr cycle seems to be related to the separation between the Maunder minimum with a center at 1685 and the so-called Dalton minimum centered at 1810. The 200-yr cycle might be related to the separation between the Dalton minimum and the deep degradation around 2000. Those cycles are similar to the 130 and 208-yr cycles in the RSSN. The amplitudes of the 120 and 200-yr cycles are great. We can think that such significant local cycles should contribute to the Attolini (130-yr) and Suess/de Vries (208-yr) or other long-term cycles during the Holocene. If a local cycle carves the deep and wide faults on the local SSN series, this will affect the spectrum for the whole time. Thus we can consider the 130 and 208-yr cycles to be related to the grand minima or grand maxima.

As we can see in Fig. 8, in a spectrum of the random signal the short cycles are weak and the long cycles are strong. This seems to be conditional, but can be seen very often. We have seen the similar behavior in the

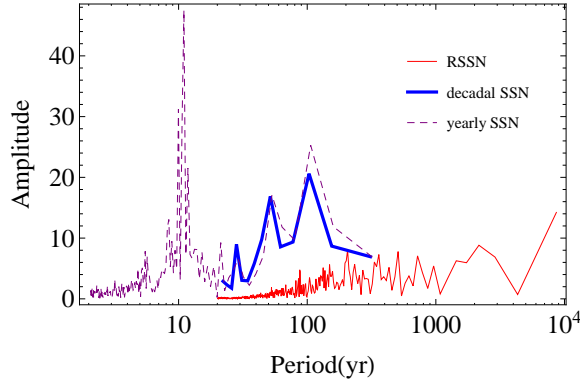


Figure 8: Comparison of the amplitude spectra between the RSSN (red) and 10-yr averaged modern SSN (blue thick). For reference, the amplitude spectrum of the yearly modern SSN is shown (purple dashed).

Table 1: The stable long-term solar cycles

Data	Stable cycles
RSSN	50~60, 85~90, 110~130, 160~200~220 <sup>a</sup> , 270, 320~350~380, 510~550, 730, 980, 1100~1200, 1350~1500, 2100~2300, 3000~3400-yr
RTSI	50~60, 85~90, 110~130~140, 190~210, 260~270, 320~350~380, 440~510~580, 750~780, 980~990~1100, 1350~1550, 2100~2500, 3100~3500, 4000~4500-yr
Modulation for RSSN and RTSI	1300~1700-yr by 2900-yr, 650~800-yr by 2500-yr, 340~390-yr by 2750-yr, 260~340-yr by 4300 and 1500-yr, 230~260-yr by 2100 and 1100-yr, 160~230-yr by 2900-yr and 730-yr, 145~160-yr by 1050-yr, 100~115-yr by 4300-yr, 90~100-yr by 2900-yr and 800-yr, 70~75-yr by 2900-yr, 20~340-yr by 500-yr
Yearly SSN	3.2~3.5, 5~6, 8, 10~11~12, 13.5~15.5, 19, 21~22, 24, 28~35, 48~53, 80~100-yr
Yearly GSN	3.2~4, 5.5~6, 8~9, 10~11, 13.5~15.5, 18~19, 22, 30~31, 41~42, 52~60~68, 88~95, 120~130, 180~190-yr
Modulation for SSN and GSN	22~25-yr by 87-yr, 13~14-yr by 93-yr, 7~9-yr by 52-yr, 5~7-yr by 21-yr

<sup>a</sup> Three peaks of cycles seem to be linked.

variation of power in the averaging down sampling: the shorter cycles depressed and the longer cycles amplified. This is for the stationary sinusoidal signal. In a random signal we have another possibility for this phenomenon. While the grand extremes form the long-term or mid-term spurious cycles, the short-term spurious cycles are least formed by those grand extremes, because the short cycle implies noisy and the random means the rare. So the energy of signal is falsely concentrated to the mid-term or long-term cycles. Thus we can see the weak short cycles in any spectrum. This effect appears not only in the power but the Fourier transform of signal.

To summarize, the stable long-term solar cycles are listed in Table 1.

### 3 The stable short-term solar cycles

We expand our discussion to the short-term solar cycles. Until now, a few short-term cycles including the Dicke's 27-day cycle have been reported: the 154-day and quasi-biennial cycles in Hathaway (2015). To find the stable short-term cycles, we inspect the monthly and daily records of the modern solar activity.

First, we analyze the monthly datasets of SSN and GSN: the monthly SSN<sup>5</sup> and the monthly GSN<sup>4</sup>. Some records in the monthly GSN have been missed so we adopt the Lomb-Scargle periodogram into the samplogram analysis. In fact, the monthly records can be considered an unevenly sampled even with variation of the length of months and the Lomb-Scargle periodogram has several advantages, one of which is capability to treat unevenly sampled data. The Lomb-Scargle samplogram and the SnD stability of cycle are shown in Fig. 9(a). The stable cycles are found to be similar to ones for the yearly datasets. And the time stability of cycle is shown in Fig. 9(b). The wavelet analysis requires the evenly sampled dataset so we take the GSN dataset since 1800/01

<sup>5</sup> The dataset is available at <http://www.ngdc.noaa.gov/stp/space-weather/solar-data/solar-indices/sunspot-numbers/international/>. The dataset covers the period from 1749/01 to 2015/05.



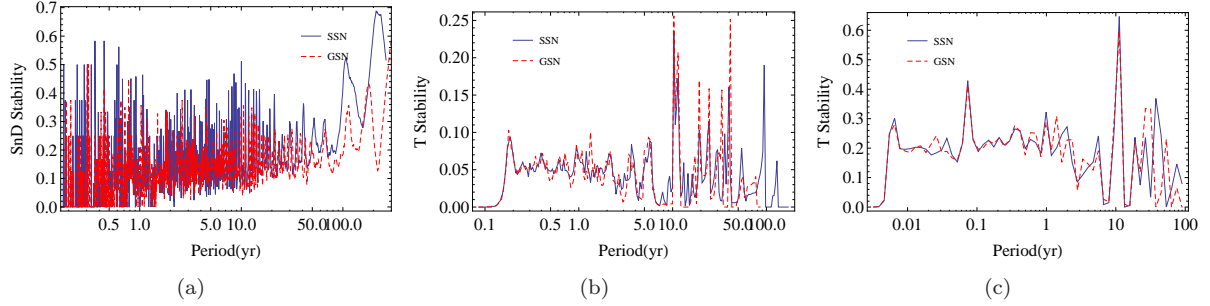


Figure 9: The SnD stability in the Lomb-Scargle samplogram (a), the time stability of the cycles for the monthly SSN and GSN (b) and the time stability of the cycles for the daily SSN and GSN (c). In wavelet scalogram we used the Morlet basis and the number of voices per octave is set 20 in (b) and 4 in (c).

and neglect the variation of the length of month in year.

We also analyze the daily SSN and GSN datasets<sup>6</sup> (Fig. 9c). The daily datasets include many missed records so we limited from 1850/01/01. The SnD stability needs a great computing capability so we evaluate only the time stability and set the number of voices per octave in wavelet analysis is set 4. The stable cycles are listed in Table 2.

Table 2: The stable short-term solar cycles

Data	Stable cycles
Monthly SSN and GSN	0.4, 0.65, 0.9~1.2, 1.9~2.1, 3.3~3.7, 5~5.5, 10~11, 16~17, 19~21~24, 30, 35, 40, 55-yr
Daily SSN and GSN	13.5, 27, 53.8-day, 0.21, 0.35, 0.59, 0.99, 1.98, 5.6, 11.2, 18.9, 26.7, 75.4-yr

In Table 2 we can find an interesting thing that the orbital periods of the planets appear approximately in the stable solar cycles: 0.25 (Mercury), 0.6 (Venus), 1.0 (Earth), 1.9 (Mars), 11.8 (Jupiter) and 29.5 yr (Saturn) are the sidereal orbital cycles of the planets (26.7-yr for the daily datasets seems to be related to the low resolution of long period). Also other origins are implied. Planetary tidal forcing of the solar activity has been proposed long ago. The current state of the theory has some problems. Some authors tried to explain solar cycles in terms of the complex arithmetic of the orbital periods of the planets (Abreu et al., 2012; Scafetta & Wilson, 2013; Solheim, 2013; Wilson, 2013). If the solar cycles would be really related to the opposition or conjunction of the planets, we have to find the orbital periods of the planets themselves in the spectrum of solar activity because the Fourier analysis decomposes an arbitrary signal into the linear series of the elementary sinusoidal cycles. Only the 11-yr cycle is discussed in relation with the Jupiter. The other cycles are negligible in spectrum or engulfed in the noisy background (for example, refer to Fig 10a for the monthly GSN). However, we saw that those cycles are existing and furthermore stable.

Is the “coincidence” between the stable solar cycles and orbital periods of the planets fortuitous? To test this “coincidence”, we compare the power of stable cycles cycles in power spectrum with the tidal force of the planets exerting on the Sun. The tidal force can be determined by the mass of the planet divided by the cube of orbital radius of the planet. Figure 10(b) shows the relation between the tidal force of the planets and the power of the those stable solar cycles that are equal to the orbital periods for the monthly datasets. The tide is in unit of the mass of the earth divided by the cube of astronomical unit. The power for the Uranus’s orbital period is roughly estimated from the Gleissberg cycle in the reconstruction dataset (refer to § 2.4). We can see that the relation for the Mars, Jupiter and Saturn is almost on a straight line. The best linear fit model for the log-log diagram in Fig. 10(b) via the least-square method is  $(1.08 \pm 0.73)x - (3.72 \pm 2.55)$  for the monthly SSN and  $(0.89 \pm 0.31)x - (3.84 \pm 1.09)$  for the monthly GSN, where  $x$  stands for  $\ln(\text{tidal force})$  and  $\pm$  means  $1\sigma$  confidence level (C.L.). We can see that three planets (Mars, Jupiter and Saturn) are completely within  $1\sigma$  C.L. about the linear model with slope of 1. The GSN dataset shows a narrower variance, but even in this case those planets are included within  $1\sigma$ C.L. This could be an implication partially of that the solar activity might have an influence proportional to the first power of the planetary tidal force. If we suppose that the Gleissberg cycle should have other origin (such as the modulation in § 2.3) but the Uranus, we can think that the Uranus could follow the rule.

<sup>6</sup> The datasets are available at the same webpages as the monthly datasets. The SSN dataset covers the period from 1818/01/01 to 2013/12/31. The GSN dataset covers the period from 1610/01/01 to 1995/12/31.

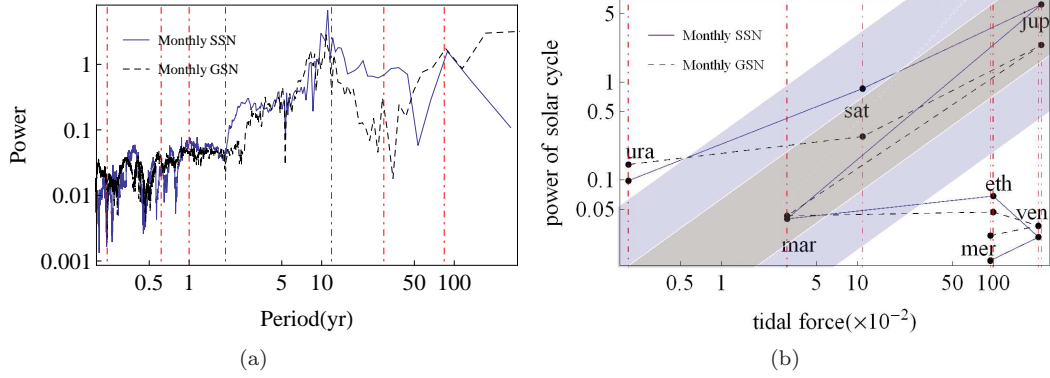


Figure 10: The power spectrum (a) and the relation between the power of the solar cycles and the tidal force of the planets that have the same orbital periods as the solar cycles (b) for the monthly SSN and GSN. The dashdotted lines stand for the sidereal orbital periods in (a) and tidal forces of the planets in (b). In (b) the power of cycles are extracted from the power spectrum (a) and the tidal force is determined to be the planetary mass in unit of the Earth’s mass divided by the cube of orbital radius in unit of astronomical unit. The power for the Uranus’s orbital period (84 yr) is estimated from the Gleissberg cycle in the reconstruction datasets. The shaded bands stand for the  $1\sigma$ C.L. about the linear relation with slope of 1: the broader one for the monthly SSN and the narrower one for the monthly GSN.

Table 3: The stable solar cycles

13.5, 27, 54-day, $\sim 0.2$ , $\sim 0.4$ , $\sim 0.6$ , $\sim 1$ , $\sim 2$ , $\sim 3.5$ , $\sim 5.5$ , $\sim 11$ , $\sim 22$ , $\sim 30$ , $\sim 50$ , $\sim 90$ , $\sim 130$ , $\sim 210$ , $\sim 270$ , $\sim 350$ , $\sim 530$ , $\sim 750$ , $\sim 1000$ , $\sim 1400$ , $\sim 2200$ and $\sim 3200$ -yr
---

In Fig. 10(b) we can see that the influences of the Mercury, Venus and Earth are estimated to be negligible, on the contrary to the traditional “V(enus)-J(upiter)-E(arth)” mechanism, which represent the strongest tidal force. This may come from that their orbital cycles are completely involved in the noisy region or that they are closer to the Sun so that they have shorter orbital period. Or this may be related to the fact that the short cycles seem to be weak in a spectrum, as we announced in § 2.4. Another problem is the period lag such as the difference between the 11-yr cycle and the orbital cycle of the Jupiter. Of course, the relation between the spectral power and the tidal force, involving only a few planets, lacks the sufficient argument for the planetary forcing, and this could be even against. However, the appearance of the near-orbital cycles for each of 6 planets upto the Saturn is clearly beyond a probable fortune. In fact, Dicke (1978) announced the super-stability of the 11-yr cycle, which is difficult to be explained by the dynamo model. The planetary force might act on the deep layer of the Sun such as a overshoot layer or exert only on the surface phenomena such as sunspot or solar flare reported by Hung (2007). Even the dynamo model depends on some specific initial data such as the differential rotation that origin is not clear yet.

## 4 Conclusion

In this paper, we chose the stable solar cycles in terms of the sampling and differencing stability in samplogram, the time stability or stationarity in wavelet scalogram and the modulation analysis. A consistency between various analyses shows that the quasi-stationary or intermittent cycles are SnD stable and that the spurious cycle is originated also from the non-stationarity of solar activity. We compare the various datasets of solar activity: the cosmogenic reconstructions, yearly, monthly, daily SSN and GSN. To summarize, we propose the stable or quasi-stationary solar cycles in Table 3. There we can see some harmonics and subharmonics such as 13.5, 54-day,  $\sim 3.5$  and  $\sim 5.5$ -yr. And some sidewaves seem to be included: for example,  $\sim 2200$  and  $\sim 3200$ -yr imply the variation of period for the Hallstatt cycle. The 8 and 13-yr cycles seem to be the transient sidewaves for the 11-yr cycle so that they are removed. The  $\sim 1100$ -yr cycle seems to be a sidewave of the Eddy cycle or harmonic of  $\sim 2200$ -yr cycle. More importantly, the spurious cycles might be involved in the Table. The rise and fall of random signal could seem to be a stationary cycle, which will be manifested by the further accumulation of data. Note that the long-term cycles extracted from the reconstructed datasets during the Holocene have not compared with a longer-period dataset, which makes their stability less certain.

Among those stable cycles we can find the near-orbital cycles of 6 planets upto the Saturn and even 84 yr for the Uranus. This may imply the possible planetary forcing of solar activity. In fact, the planetary influence on the solar activity is inevitable. It is only matters how the intensity is and what the mechanism is. Furthermore, we have found a linear proportionality between the tidal force and the power of corresponding cycles in spectrum, though for a few planets. The power of shortest or longest cycles of planets might be biased because in spectrum of a random signal the short cycle might be depressed and the long cycle amplified via various pre-manipulations such as the averaging. The planetary forcing means an extrinsic origin of the solar activity while the dynamo mechanism corresponds to an intrinsic origin. The solar activity seems to have the various origins.

## Acknowledgements

K. Chol-jun has been supported by **Kim Il Sung** University during investigation.

## References

- Abreu, J. A., Beer, J., Ferriz-Mas, A., McCracken, K. G., Steinhilber, F., 2012, Is there a planetary influence on solar activity?, *Astronomy and Astrophysics*, 548, A88, <http://dx.doi.org/10.1051/0004-6361/201219997>
- Attolini, M. R., Galli, M., Nanni, T., 1988, Long and short cycles in solar activity during the last millennia. In Stephenson, F.R. and Wolfendale, A.W., editors, *Secular solar and geomagnetic variations in the last 10,000 years*, Dordrecht: Kluwer, 49-68
- Beer, J., Tobias, S. M., Weiss, N. O., On long-term modulation of the Sun's magnetic cycle, *Monthly Notices of the Royal Astronomical Society*, 473, 1596, <http://doi:10.1093/mnras/stx2337>
- Bond, G., Showers, W., Cheseby, M., Lotti, R., Almasi, P., deMenocal, P., Priore, P., Cullen, H., Hajdas, I., Bonani, G., A Pervasive Millennial-Scale Cycle in North Atlantic Holocene and Glacial Climates, 1997, *Science*, 278, 1257, DOI: 10.1126/science.278.5341.1257
- Chol-jun, K., 2020, Stability of cycle in samplogram and spurious cycles in solar activity, arXiv:2009.09578 [astro-ph.SR]
- Chol-jun, K., Jik-su, K., 2020, Solar activity cycle of  $\sim 200$  yr from mediaeval Korean records and reconstructions of cosmogenic radionuclides, *Monthly Notices of the Royal Astronomical Society*, 492, 384-393, <http://doi:10.1093/mnras/stz3452>
- Clette, F., Svalgaard, L., Vaquero, J. M., Cliver, E.W., 2014, Revisiting the Sunspot Number. A 400-Year Perspective on the Solar Cycle, *Space Sci. Rev.* 186, 35-103, doi: 10.1007/s11214-014-0074-2
- Dicke, R. H., 1978, Is there a chronometer hidden deep in the Sun, *Nature*, 276, 676-680
- Hathaway, D. H., 2015, The Solar Cycle, *Liv. Rev. Sol. Phys.*, 12, 4, doi:10.1007/lrsp-2015-4
- Hoyt, D. V., Schatten, K. H., 1998, Group Sunspot Numbers: A New Solar Activity Reconstruction, *Solar Phys.*, 181, 491-512, doi: 10.1023/A:1005056326158
- Hung, C. -C., 2007, Apparent Relations Between Solar Activity and Solar Tides Caused by the Planets, NASA/TM-2007-214817
- Ma, L. H., 2009, Gleissberg cycle of solar activity over the last 7000 years, *New Astronomy*, 14, 1-3, doi:10.1016/j.newast.2008.04.001
- Petrovay, K., 2010, Solar Cycle Prediction, *Liv. Rev. Sol. Phys.*, 7, 6, <http://www.livingreviews.org/lrsp-2010-6>
- Solanki, S. K., Usoskin, I. G., Kromer, B., Schüssler, M., Beer, J., 2004, Unusual activity of the sun during recent decades compared to the previous 11,000 years, *Nature*, 431, 1084

- Steinhilber, F., Abreu, J. A., Beer, J., Brunner, I., Christl, M., Fischer, H., Heikkilä, U., Kubik, P. W., Mann, M., McCracken, K. G., Miller, H., Miyahara, H., Oerter, H., Wilhelms, F., 2012, 9,400 years of cosmic radiation and solar activity from ice cores and tree rings, PNAS, 109, 5967, <http://www.pnas.org/cgi/doi/10.1073/pnas.1118965109>
- Scafetta, N., Wilson, R. C., 2013, Empirical evidences for a planetary modulation of total solar irradiance and the TSI signature of the 1.09-year Earth-Jupiter conjunction cycle, Astrophysics and Space Science, 346, 2, DOI: 10.1007/s10509-013-1558-3
- Solheim, J. -E., 2013, The sunspot cycle length - modulated by planets?, Pattern Recognition in Physics, 1, 159-164, doi:10.5194/prp-1-159-2013
- Usoskin, I. G., 2008, A History of Solar Activity over Millennia, Living Review of Solar Physics, 5, 3, <http://www.livingreviews.org/lrsp-2008-3>
- Usoskin, I. G., Gallet, Y., Lopes, F., Kovaltsov, G. A., Hulot, G., 2016, Solar activity during the Holocene: the Hallstatt cycle and its consequence for grand minima and maxima, Astronomy and Astrophysics, 587, A150, arXiv:1602.02483v1 [astro-ph.SR]
- Wilson, I. R. G., 2013, The Venus-Earth-Jupiter spin-orbit coupling model, Pattern Recognition in Physics, 1, 147-158, doi:10.5194/prp-1-147-2013
- Wu, C. J., Usoskin, I. G., Krivova, N., Kovaltsov, G. A., Baroni, M., Bard, E., Solanki, S. K., 2018, Solar activity over nine millennia: A consistent multi-proxy reconstruction?, Astronomy and Astrophysics, 615, A93, <https://doi.org/10.1051/0004-6361/201731892>